NANO LETTERS

pubs.acs.org/NanoLett Letter

Subtherapeutic Photodynamic Treatment Facilitates Tumor Nanomedicine Delivery and Overcomes Desmoplasia

Marta Overchuk, Kara M. Harmatys, Shrey Sindhwani, Maneesha A. Rajora, Adam Koebel, Danielle M. Charron, Abdullah M. Syed, Juan Chen, Martin G. Pomper, Brian C. Wilson, Warren C. W. Chan, and Gang Zheng*

Cite This: *Nano Lett.* 2021, 21, 344−352 Read Online

ACCESS | Metrics & More | Article Recommendations | Supporting Information

ABSTRACT: Limited tumor nanoparticle accumulation remains one of the main challenges in cancer nanomedicine. Here, we demonstrate that subtherapeutic photodynamic priming (PDP) enhances the accumulation of nanoparticles in subcutaneous murine prostate tumors ∼3−5-times without inducing cell death, vascular destruction, or tumor growth delay. We also found that PDP resulted in an ∼2-times decrease in tumor collagen content as well as a significant reduction of extracellular matrix density in the subendothelial zone. Enhanced nanoparticle accumulation combined with the reduced extravascular barriers improved therapeutic efficacy in the absence of off-target toxicity, wherein 5 mg/kg of Doxil with PDP was equally effective in delaying tumor growth as 15 mg/kg of Doxil. Overall, this study demonstrates the potential of PDP to enhance tumor nanomedicine accumulation and alleviate tumor desmoplasia without causing cell death or vascular destruction, highlighting the utility of PDP as a minimally invasive priming strategy that can improve therapeutic outcomes in desmoplastic tumors.

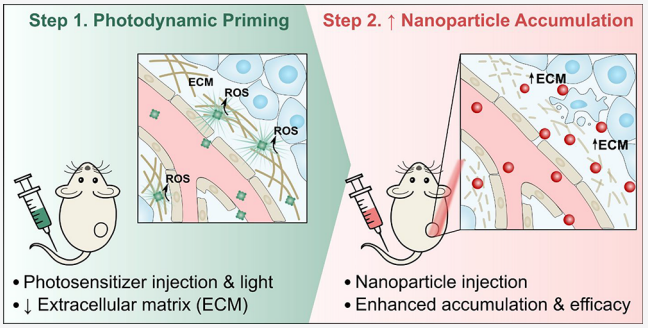

KEYWORDS: *photodynamic therapy, prostate cancer, nanomedicine, PSMA, extracellular matrix*

Since the discovery of the enhanced permeability and retention effect,[1,2] tremendous preclinical and clinical efforts have been directed toward the development and clinical translation of drug-carrying nanoparticles for cancer treatment.[3] However, despite the significant advances in the field of nanomedicine, a recent meta-nalysis found that only about 0.7% (median) of the nanoparticle injected dose reaches solid tumors.[4] While the nanoparticle's synthetic (size, shape, surface charge) and biological (protein corona, clearance rate) characteristics undoubtedly play an important role in determining its fate *in vivo*,[5] the local tumor microenvironment barriers, such as suboptimal tumor vascular density/perfusion,[6] elevated interstitial fluid pressure,[7] and desmoplasia,[8] are unlikely to be addressed by purely changing nanoparticle design. In addition to the limited bulk tumor nanoparticle accumulation, its poor tumor penetration contributes to insufficient cancer cell-drug exposure, resulting in resistance.[9] This issue is particularly prominent in highly desmoplastic tumors such as pancreatic ductal adenocarcinoma.[10] As the field's understanding of tumor pathophysiology has progressed, it has become clear that in addition to advanced nanoengineering approaches, new biological strategies might be required to solve the tumor nanomedicine delivery challenge.[11−13]

One way of overcoming tumor delivery barriers is to pair nanomedicines with "priming" strategies that can modulate the hostile tumor microenvironment and enable effective tumor nanomedicine accumulation and/or intratumoral distribution.[14,15] Radiation, ultrasound, and enzymatic degradation of the tumor extracellular matrix have all been explored for this purpose.[14,15] Ideally, such a priming modality would require a high degree of spatial control, allowing for enhanced nanomedicine accumulation at the tumor site, but not in the surrounding healthy tissue, as well as a nonoverlapping toxicity profile with chemotherapy. Photodynamic therapy (PDT), which activates photosensitizers with light to locally generate cytotoxic reactive oxygen species, readily meets these criteria.[16−18] Indeed, several studies demonstrated that PDT can be employed as a means of enhancing tumor accumulation of various types of nanoparticles−a phenomenon that has been termed photodynamic priming (PDP).[19−22]

Received: September 14, 2020
Revised: November 22, 2020
Published: December 10, 2020

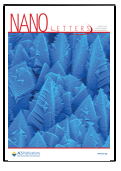

https://dx.doi.org/10.1021/acs.nanolett.0c03731
Nano Lett. 2021, 21, 344−352

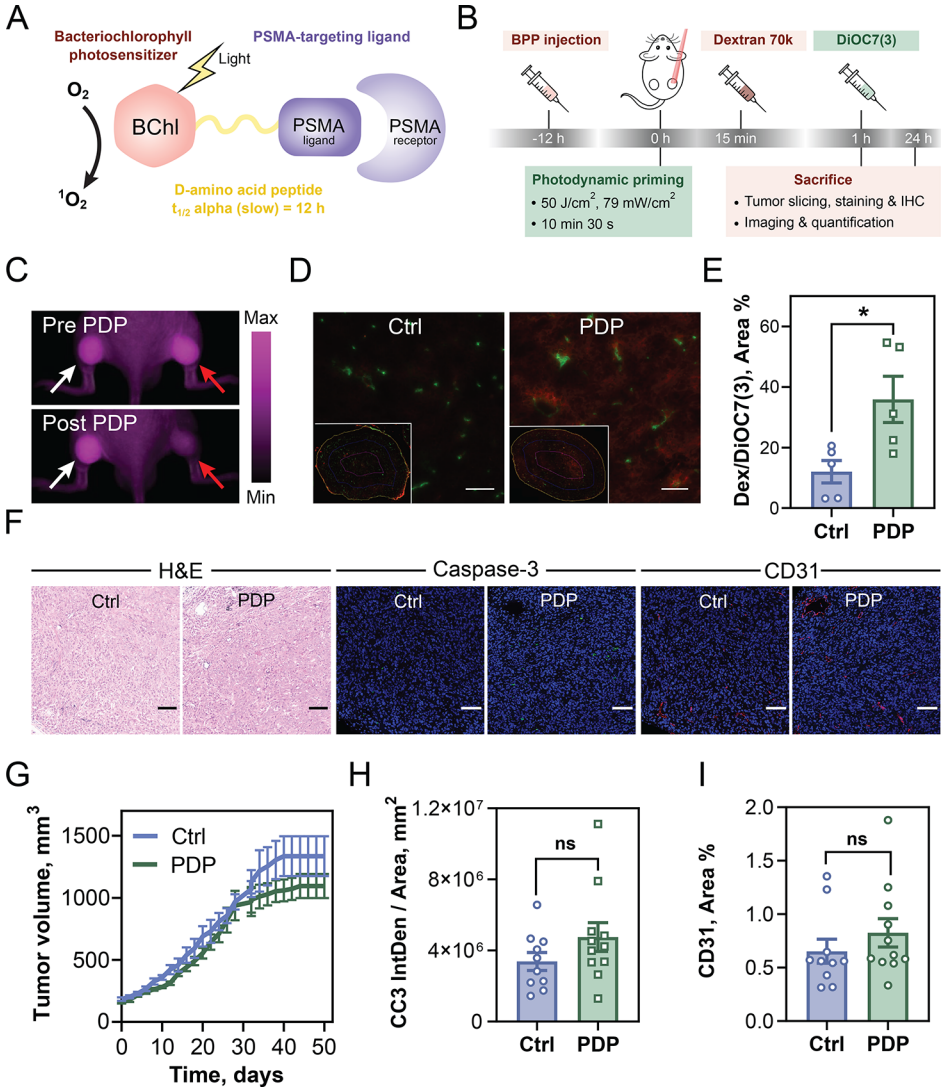

Figure 1. Subtherapeutic PSMA-targeted photodynamic priming (PDP). (A) Bacteriochlorophyll-peptide-PSMA (BPP) schematic. Bacteriochlorophyll provides potent PDT activity upon 750 nm light irradiation. The 9 amino acid peptide imparts a long plasma circulation time, and the conjugated PSMA targeting ligand maintains high-affinity ligand binding. (B) General PDP workflow. (C) Hyperspectral fluorescence imaging of BPP in a mouse bearing dual PSMA+ PC3 PIP tumors at 12 h postadministration (top) and immediately after PDP. The right tumor (red arrow) was treated with PDP, and the left tumor (white arrow) was used as a dark control. (D) Representative dextran fluorescence in a dark control and PDP-treated tumor slices at 1 h postinjection. Red − Texas Red; Green − DiOC7. (E) Quantification of dextran-positive areas in whole-tumor sections normalized by DiOC7(3) area. (F) Representative H&E, cleaved caspase 3 (CC3) and CD31-stained sections in the dark control and PDP-treated tumors 24 h postlaser treatment. (G) Tumor growth curves in the control and PDP-treated mice. (H) CC3 fluorescence integrated density quantification and (I) CD31% area quantification in the dark control and PDP-treated tumors (mean ± S.E.M., n = 10−11, each dot on the graph represents a separate tumor, two-tailed t test, $^*P \leq 0.05$).

The most studied biological effects of PDT, vascular damage and direct cell killing, have both been studied in the context of tumor nanomedicine delivery. In their seminal study, Snyder and colleagues demonstrated that PDT using hematoporphyrin derivative can enhance the delivery and efficacy of Doxil in a murine colon cancer model.[19] Photodynamic priming was hypothesized to increase tumor vascular leakiness, resulting in the enhanced extravasation of macromolecules and nanoparticles. Indeed, the ability of PDP to permeabilize vascular barriers and increase the extravasation of Evans blue and FITC-dextran was demonstrated by using an *in vitro* endothelial permeability assay as well as intravital imaging in a MatLyLu rat prostate tumor model.[23] Such PDP-induced vascular modulation was also leveraged in more recent studies, wherein low-fluence laser irradiation was applied at early time points after photosensitizer injection to enhance the accumulation of liposomal doxorubicin and cisplatin in various rat lung cancer models.[24−27] Alternatively, targeted photodynamic cancer cell killing was explored in a study by Sano and colleagues,[28−31] who proposed the use of targeted photosensitizer-antibody conjugates to enhance the delivery of various nanoparticles, which was termed photoimmunotherapy. It was hypothesized that photoimmunotherapy facilitates tumor nanomedicine delivery by inducing localized cell death in the subendothelial area, thereby decreasing solid tissue stress, dilating tumor vessels, and enhancing nanoparticle extravasation.[29]

While cytotoxic and antivascular PDT effects are well-known, PDP can also exert a variety of molecular, physical, and biological effects that enhance the efficacy of other modalities

https://dx.doi.org/10.1021/acs.nanolett.0c03731
Nano Lett. 2021, 21, 344−352

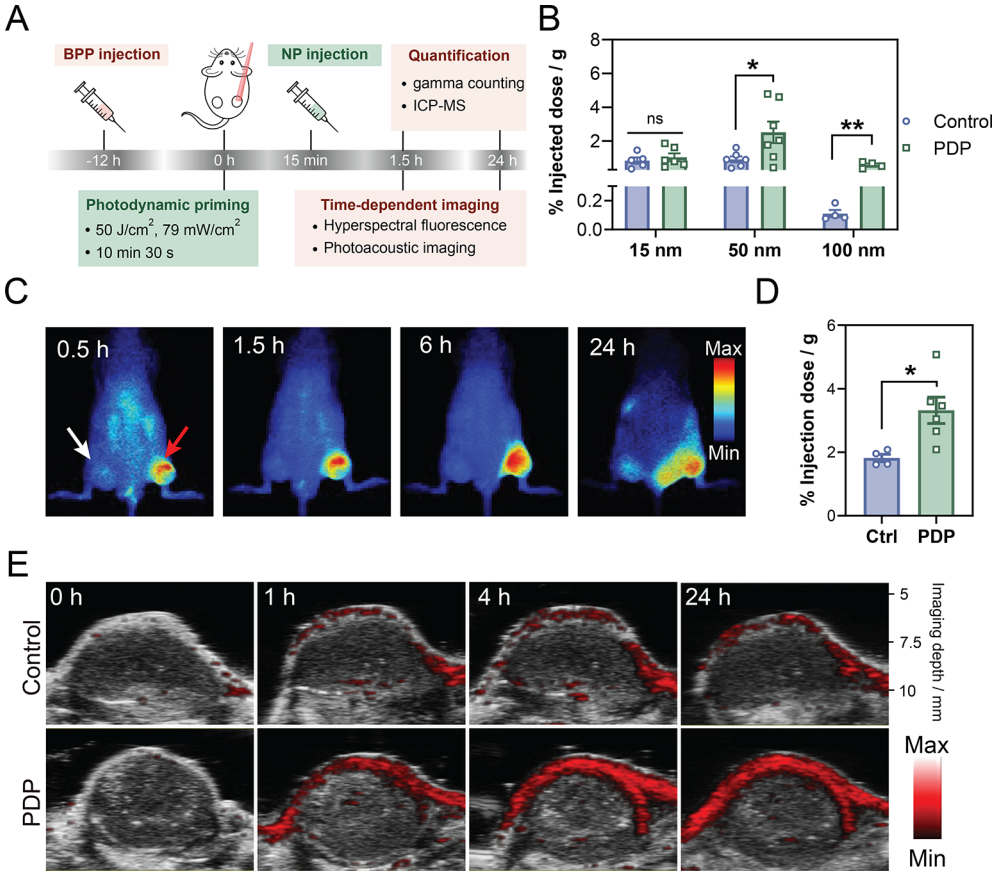

Figure 2. PDP-enhanced tumor accumulation of various organic and inorganic nanoparticles. (A) Schematic representation of the PDP-enabled nanoparticle delivery workflow. (B) ICP-MS quantification of 15, 50, and 100 nm gold nanoparticles (AuNPs) in the dark control and PDP-treated tumors (mean ± S.E.M., n = 4−6, each dot on the graph represents a separate tumor, two-tailed t test, $^*P \leq 0.05$). (C) Representative hyperspectral fluorescence images of a mouse bearing dual subcutaneous prostate PSMA + PC3 PIP tumors intravenously injected with 40 nmol of PEGylation-free lipoprotein porphyrin nanoparticles (PLP) at 0.5, 1.5, 6, and 24 h postinjection (n = 3). The right tumor (red arrow) was treated with PDP 15 min prior to PLP injection, and the left tumor (white arrow) was used as a dark control. (D) ^{64}Cu-PLP quantification in the dark control and PDP-treated tumors at 1.5 h postinjection (mean ± S.E.M., two-tailed t test, each dot on the graph represents a separate tumor). (E) Representative time-dependent photoacoustic imaging in a dual subcutaneous PSMA+ PC3 PIP prostate tumor-bearing mouse (n = 3) intravenously injected with PA-liposomes 15 min post-PDP.

such as immunotherapy, chemotherapy, or VEGF inhibition.[32−34] The exact biological mechanism of PDP is not fully established, but several studies demonstrated that it can target various tumor microenvironment components. PDP increases tumor immunogenicity and permeability as well as affects its transcriptomic, proteomic, and metabolomic landscapes.[32,35] In a recent study by Huang et al., it was discovered that PDT decreases the expression of stemness markers (CD44 and CXCR4) in a preclinical pancreatic cancer model, thereby overcoming resistance development during multicycle chemotherapy.[20] A follow-up study demonstrated that PDP combined with vitamin D receptor activation can even further boost the efficacy of liposomal irinotecan.[36]

The extracellular matrix is another important tumor microenvironment component that can be targeted by PDP. In a recent study, Obaid and colleagues demonstrated that specificity-tuned EGFR-targeted benzoporphyrin-lipid nanoconstructs in combination with therapeutic PDT doses resulted in a 1.5-times decrease in pancreatic tumor collagen deposition.[37] This finding opened multiple research avenues regarding the mechanism of this effect, as well as its potential impact on tumor nanomedicine accumulation. Specifically, it remains unclear whether the observed collagen photomodulation stems from the significant PDT-induced necrosis/cancer cell and cancer-associated fibroblast death or is an independent and previously unexplored PDT effect. Given the established role of desmoplasia in the limited extravasation and penetration of nanomedicine in tumors,[8,38,39] it is likely that such collagen photomodulation can be utilized to facilitate tumor nanomedicine accumulation.

In this current study, we focus on the development of a subtherapeutic PDP protocol to investigate the possibility of tumor extracellular matrix photomodulation in the absence of any significant cell death. In our study, we employed a prostate-specific membrane antigen (PSMA)-targeted bacteriochlorophyll photosensitizer (BPP; Figure 1A) in a subcutaneous PSMA+ PC3 PIP prostate tumor mouse model.[40] This long-circulating agent ($t_{1/2\ slow}$ = 12.0 h) was chosen for its effective tumor accumulation,[40] photosensitizing properties, and low molecular weight (MW < 2 kDa) that allows for its tissue penetration. Subtherapeutic PDP enhanced the delivery of various organic and inorganic nanoparticles, including Doxil, leading to its improved therapeutic efficacy. Furthermore, we quantitatively characterized the effects of subtherapeutic PDP on the tumor extracellular matrix content and ultrastructure,

https://dx.doi.org/10.1021/acs.nanolett.0c03731
Nano Lett. 2021, 21, 344−352

which provided a new rationale for PDP application in desmoplastic tumors.

RESULTS AND DISCUSSION

Photodynamic Priming Enhances Tumor Vascular Leakiness. We previously described the synthesis, characterization, and PDT efficacy of the PSMA-targeted long-circulating bacteriochlorophyll-based photosensitizer (BPP) (Figure S1).[40] BPP in combination with therapeutic light fluences (125 J/cm^2 at 750 nm) induced destruction of subcutaneous PSMA+ PC3 PIP tumors. Next, we explored the possibility of utilizing this agent in combination with a much lower fluence (50 J/cm^2) as a priming strategy to enhance the delivery of macromolecular agents to the tumor (Figure 1B). Mice bearing dual subcutaneous PSMA+ PC3 PIP tumors were intravenously injected with 50 nmol BPP, and 12 h later one tumor was irradiated with 50 J/cm^2 laser light (Figure 1C). Fifteen minutes post-PDP, animals were injected with dextran (70 000 MW) fluorescently labeled with Texas Red, which circulated for another hour. Immediately before euthanasia, animals were injected with DiOC7(3) dye to mark patent vessels. Quantification of the dextran-positive area demonstrated an ∼2-times increase in dextran extravasation in the PDP-treated tumors (Figure 1D and E). No statistically significant difference was detected in the DiOC7(3)-positive area between the dark control and PDP-treated tumors, suggesting that PDP did not change the area of the patent vasculature (Figure S2).

Subtherapeutic PDP Does Not Result in Significant Cell Death or Vascular Destruction. Given the strong photosensitizing properties of BPP, we investigated the extent of cellular and vascular damage exerted by PDP. Hematoxylin and eosin staining demonstrated no signs of tissue necrosis 24 h post-PDP (Figure 1F). Furthermore, PDP had no influence on the tumor growth kinetics (Figure 1G). Fluorescence quantification of the cleaved caspase 3 (CC3) in whole-tumor sections demonstrated no significant increase in cell apoptosis (Figure 1F and H), which was further confirmed by the lack of TUNEL staining in the PDP-treated tumors (Figure S3). CD31 immunohistochemistry demonstrated no change in vascular area 24 h following PDP (Figure 1F and I). While this PDP protocol likely elicited some transient changes in vascular leakiness, it did not compromise tumor vasculature, potentially enabling the repeated systemic drug/nanomedicine administration. Furthermore, no significant change was detected in the tumor macrophage infiltration as quantified by F4/80 immunohistochemistry (Figure S4). Histological evidence together with the lack of tumor growth delay in the PDP-treated animals (Figure 1G) validated the selected combination of BPP dose and light fluence is subtherapeutic.

PDP Facilitates Tumor Accumulation of Organic and Inorganic Nanoparticles. Once we established PDP's ability to enhance dextran extravasation, we explored its application as a priming strategy to facilitate the delivery of various nanoparticle types. Mice bearing bilateral PSMA+ PC3 PIP tumors were subjected to PDP as described above, followed by the injection of one of the nanoparticle types including gold nanoparticles (AuNPs), PEGylation-free lipoprotein porphyrin nanoparticles (PLP),[41] and photoacoustic liposomes (PA-liposomes)[42] followed by imaging and quantification (Figure 2A). After the injection of high doses of gold nanoparticles (Table S1), a significant change in animal skin color was observed (Figure S5). Interestingly, skin covering the PDP-treated tumor turned visibly darker compared to the contralateral side, suggesting that vascular leakiness was increased locally at the irradiated site as early as 1 h postinjection (Figure S5). Gold nanoparticles circulated for 24 h, then animals were euthanized by transcardial perfusion, tumors and major clearance organs were excised and weighted, and gold content was quantified using inductively coupled plasma mass spectrometry (ICP-MS) (Figures 2B and S6). PDP treatment resulted in an enhanced tumor accumulation of 50 and 100 nm gold nanoparticles by 3- and 5-times, respectively (Figure 2B). While no change in tumor accumulation of the 15 nm nanoparticles was observed at 24 h post-PDP, it should be noted that tumor accumulation data at a single time point may not capture the dynamic changes in the nanoparticle delivery kinetics. Additionally, these data could be explained by the fact that 15 nm particles, due to their smaller size, penetrate into the tumor tissue more effectively compared to the 50 and 100 nm, as previously shown by Sykes et al.;[43] therefore, they may not further benefit from PDP. It would be interesting to further investigate the size effects of nanoparticle tumor accumulation post-PDP treatment at different time points as well as PDP effects on the nanoparticle extravasation distance.

Next, we investigated time-dependent accumulation of PEGylation-free lipoprotein porphyrin nanoparticles (PLP) (Figure S7) in the dark control and treated tumors using hyperspectral fluorescence imaging (Figure 2C). PDP-treated tumors showed a strong PLP fluorescence signal as early as 30 min after nanoparticle injection. The PLP fluorescence signal continued to increase up to 24 h post injection, while PLP fluorescence at the dark control tumor site only started to appear. While we observed a notable increase in PLP fluorescence at the early time points, it was unclear if it was a result of faster nanoparticle disruption and fluorescence signal unquenching or increased PLP tumor accumulation. To clarify if this time-dependent signal enhancement in PDP-treated tumors was coming from the PLP tumor accumulation rather than from nanoparticle disruption and fluorescence activation, we employed ^{64}Cu-radiolabeling of PLPs. Ten mice bearing single PSMA+ PC3 PIP tumors were injected with 50 nmol of BPP 12 h prior to the experiment. Six out of ten animals were subjected to PDP priming, and four animals were left untreated prior to injection of ^{64}Cu-labeled PLPs (Figures 2D and S8). Nanoparticles circulated for 1.5 h, and then animals were euthanized by transcardial perfusion to wash out the remaining ^{64}Cu-PLP radioactivity from circulation. Tumors and major organs were excised and weighed, and nanoparticle injected dose per gram (%ID/g) was quantified using a gamma counter. PDP treatment enhanced PLP tumor accumulation from ∼2%ID/g to ∼3.5% ID/g at 1.5 h post injection (Figure 2D).

Finally, we utilized photoacoustic liposomes (PA-liposomes) to evaluate if PDP can deliver intact liposome-like nanoparticles to the tumor or rather facilitate the delivery of their dissociated building blocks. PA-liposomes contain bacteriochlorophyll-lipid building blocks that exhibit a characteristic absorption band at 820 nm only present within the intact nanostructure due to J-aggregation (Figure S9). PA-liposome accumulation was monitored in the dark control and PDP-treated tumors using photoacoustic imaging that detects the 820 nm absorption band of the intact nanoparticles (Figure 2E). Similar to the PLPs, PA-liposome accumulation became visible as early as 1 h post injection in the PDP-treated tumor

https://dx.doi.org/10.1021/acs.nanolett.0c03731
Nano Lett. 2021, 21, 344−352

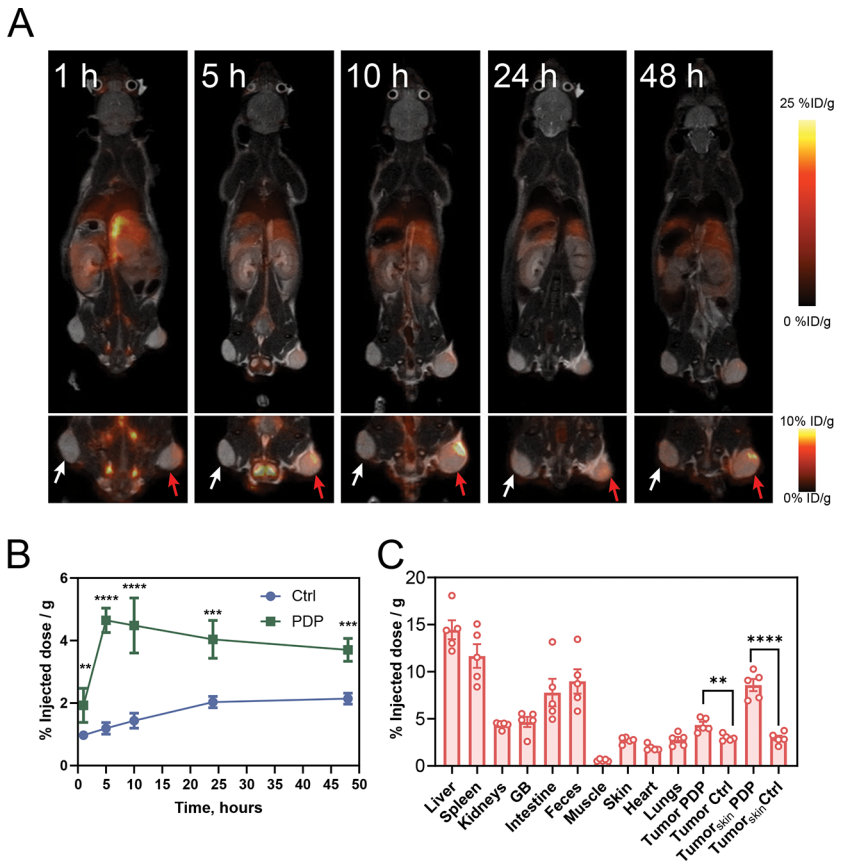

Figure 3. PDP-enabled ^{64}Cu-liposome accumulation. (A) Representative PET-MRI imaging of ^{64}Cu-liposome accumulation in a dual subcutaneous PSMA+ PC3 PIP prostate cancer model. The tumor on the right was treated with PDP 15 min prior to the ^{64}Cu-liposome injection, and the tumor on the left was left untreated as a dark control. (B) ^{64}Cu-liposome accumulation in the dark control and treated tumors represented as the % of the injected dose per g (%ID/g) at the different time points over the course of 48 h. (C) ^{64}Cu-liposome biodistribution in the tumor and the major organs at 48 h postinjection quantified using gamma counting (mean ± S.E.M., n = 5, two-tailed t test, $^{**}P \leq 0.01$; $^{***}P \leq 0.001$; $^{****}P \leq 0.0001$).

and continued to increase up to 24 h, while the contralateral tumor had only minor PA-liposome uptake at all time points attributed to passive accumulation. Collectively, these data demonstrate that PDP can enhance tumor accumulation of various types of organic and inorganic nanoparticles.

PDP Increases Tumor AUC of ^{64}Cu-Liposomes. After establishing that subtherapeutic PDP can enhance the delivery of various nanoparticle types, we investigated how PDP changes liposomal tumor pharmacokinetics (Figure 3). Five animals bearing dual subcutaneous PSMA+ PC3 PIP tumors were subjected to PDP and administered ∼100 nm ^{64}Cu-labeled liposomes (Figure S10). Mice were imaged using the PET-MRI system at 1, 5, 10.5, 24, and 48 h (Figure 3A) and then euthanized by transcardial perfusion. ^{64}Cu-liposome %ID/g was quantified in the dark control and PDP-treated tumors as well as in major clearance organs. ^{64}Cu-liposome tumor AUCs were determined by quantifying the radioactivity at all time points using Inveon software (Figure 3B). Similar to what we observed using optical imaging with lipoprotein-like nanoparticles and PA-liposomes, ^{64}Cu-liposome %ID/g was higher in PDP-treated tumors at all time points (Figure 3A and B). Specifically, ^{64}Cu-liposome accumulation reached its peak at 5 h (4.65 ± 0.20%ID/g) in PDP-treated tumors, followed by a gradual decrease until 48 h postinjection (3.70 ± 0.18%ID/g). In the control tumors, ^{64}Cu-liposome accumulation gradually increased until 24 h (2.03 ± 0.08%ID/g), after which it remained constant until 48 h. ^{64}Cu-liposome biodistribution was quantified using gamma counting at 48 h postinjection, indicating that PDP increased ^{64}Cu-liposome tumor accumulation from 2.98 ± 0.15 to 4.34 ± 0.32%ID/g (Figure 3C and Table S2).

PDP Enhances Doxil Efficacy, Eliminating Its off-Target Toxicities. The ability of PDP to enhance the efficacy of systemic chemotherapy[19,20,36] as well as receptor tyrosine kinase inhibitor treatment[34] was previously demonstrated in the literature. Given the observed increase in the liposomal tumor accumulation following PDP, we investigated how PDP can enhance tumor Doxil accumulation and therapeutic efficacy (Figure 4A). Prior to survival studies, we conducted several preliminary experiments to confirm that the developed PDP protocol achieves maximum Doxil accumulation. First, we screened several nanoparticle injection time points post-PDP, ranging from 15 min to 24 h. Similar to the data found in the literature, 15 min post-PDP was the optimal time point for maximum Doxil accumulation (Figure S11A).[19] Next, we screened four different irradiances (50 J/cm^2 at 26, 39, 79, and 119 mW/cm^2), and 79 mW/cm^2 resulted in the highest and least variable tumor Doxil accumulation (Figure S11B).

After establishing optimal PDP settings, animals bearing dual subcutaneous PSMA+ PC3 PIP tumors were treated with PDP and administered Doxil at 2.5, 5, 10, and 20 mg/kg. Two- to three-times Doxil accumulation enhancement was found at all

https://dx.doi.org/10.1021/acs.nanolett.0c03731
Nano Lett. 2021, 21, 344−352

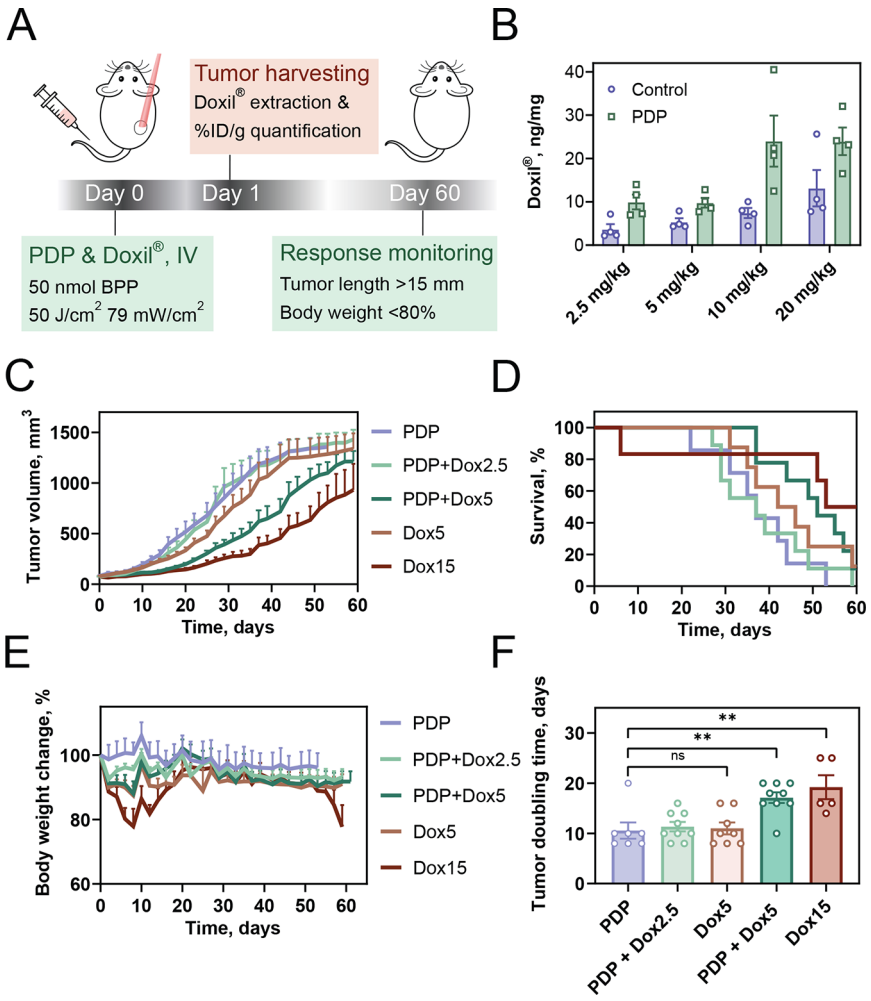

Figure 4. PDP-enhanced Doxil tumor accumulation and therapeutic efficacy. (A) Schematic representation of the enhanced Doxil delivery workflow and the survival study. (B) Doxil accumulation in the control and PDP-treated tumors 24 h post-PDP. (C) Tumor growth curves in animals treated with PDP-only, PDP + Doxil at 2.5 mg/kg (PDP + Dox2.5), PDP + Doxil at 5 mg/kg (PDP + Dox5), Doxil at 5 mg/kg, and Doxil at 15 mg/kg. (D) Survival curves, (E) relative body weight change, and (F) tumor doubling times in the same groups (mean ± S.E.M., significance was determined using one-way ANOVA, wherein all groups were compared to the PDP-only group and corrected for multiple comparisons using the Dunnett method. $^{**}P \leq 0.01$; $^{***}P \leq 0.001$; $^{****}P \leq 0.0001$).

Doxil doses (Figure 4B). To establish the Doxil dose−response relationship, mice bearing PSMA+ PC3 PIP tumors were injected with 5, 10, 15, and 20 mg/kg of Doxil, after which tumor growth kinetics and animal body weight were monitored every other day for the next 60 days (Figure S12). Doxil delayed PSMA+ PC3 PIP tumor growth in a dose-dependent manner, wherein the animals treated with 20 mg/kg demonstrated the slowest tumor growth (Figure S12A). In addition to the tumor growth delay, Doxil treatment led to significant off-target toxicities, such as skin hyperkeratosis and cachexia. In fact, while animals treated with 20 mg/kg of Doxil demonstrated the slowest tumor growth, 3 out of 6 animals had to be removed from the experiment and euthanized before day 12 of treatment due to the extreme cachexia (<80% of the initial body weight). After establishing the Doxil dose−response relationship, PDP's ability to enhance Doxil efficacy was studied (Figure 4C and D). PDP treatment combined with a single Doxil injection at 5 mg/kg (PDP + Dox5) resulted in a significantly prolonged tumor doubling time compared to PDP alone, while tumor doubling times in animals treated with 5 mg/kg of Doxil alone did not differ significantly from the PDP-only group (Figure 4F). PDP in combination with a lower Doxil injection dose (2.5 mg/kg) did not result in tumor growth delay compared to the PDP-only control. This lack of tumor growth inhibition in the PDP + Dox2.5 group is likely explained by the differences in tumor pharmacokinetics across different Doxil doses, leading to the long-lasting tumor growth inhibition at 5 mg/kg. Similar phenomenon was demonstrated in a study by Snyder et al., wherein photodynamic treatment enhanced Doxil efficacy compared to PDT only at the doses of 3−10 mg/kg, while no significant enhancement was observed at 1.25 and 2.5 mg/kg.[19] In summary, subtherapeutic PDP enhances the efficacy of liposomal doxorubicin by ∼3-times, which correlates with the 2−3-times Doxil tumor accumulation enhancement. While treatment with Doxil at 15 mg/kg produced the highest survival proportion (Figure 4D), mice in this group started to develop a second wave of cachexia at the end of the experiment (Figure 4E), indicating the long-term toxicity of this treatment. Overall, while we demonstrated the ability of PDP to enhance the efficacy of systemically administered nanomedicines, its effects on the therapeutic window need to be further investigated.

PDP Modulates the Tumor Extracellular Matrix Content and Ultrastructure. After we established PDP's

https://dx.doi.org/10.1021/acs.nanolett.0c03731
Nano Lett. 2021, 21, 344−352

ability to enhance tumor accumulation of various nanoparticles and improve Doxil therapeutic efficacy, we hypothesized that the PDP mechanism may involve modulation of the tumor extracellular matrix (ECM) content. Tumor ECM is one of the major barriers to nanoparticle extravasation and interstitial diffusion.[10,44] The effects of photodynamic therapy on the tumor extracellular matrix are not fully understood, particularly in the case of subtherapeutic light irradiation. Early ultrastructural studies indicated that PDT may induce changes in the tumor subendothelial ECM ultrastructure, but these changes have not been quantified[45] or confirmed by a secondary method, such as histological analysis.[45] In a more recent study, Obaid and colleagues reported that PDT using EGFR-targeted benzoporphyrin-containing liposomal nanoconstructs decreased collagen deposition in a pancreatic ductal adenocarcinoma mouse model.[37] Since both studies employed relatively high fluences (100 and 150 J/cm^2, respectively) that resulted in notable tumor necrosis, it remains unclear if tumor ECM photomodulation occurs at subtherapeutic fluences. Quantitative histological analysis of the whole-tumor sections stained with collagen marker Masson's trichrome revealed a nearly 2-times decrease in the collagen content 24 h after PDP compared to the dark control (Figure 5A and B).

Next, we examined the ECM ultrastructure in the subendothelial zone using transmission electron microscopy (TEM) (Figure 5C and Figure S14). Tumor microvessels consist of tubular sheets of endotheliocytes enclosed in a basement membrane. If pericytes were observed, they were either closely adherent to endotheliocytes and enclosed in the basement membrane or dispatched from the vessel due to edema. No signs of endotheliocyte damage were observed after PDP; endotheliocyte and pericyte morphology closely resembled that of control tumors. The abluminal side of endotheliocytes in dark control tumors was tightly enclosed in a basement membrane, surrounded by the extracellular matrix, consisting mainly of collagen fibers. Basement membranes, if visible, were closely tracing the outside membrane of the endotheliocytes (Figure 5C and D). In the PDP-treated tumors, microvessels were surrounded by negligible amounts of the extracellular matrix compared to the controls; basement membranes were frequently disattached from the abluminal side of endotheliocytes (Figure 5C and D). Moreover, gold nanoparticles frequently pooled in the space between the endotheliocyte and the basement membrane. To quantify change in the subendothelial ECM coverage upon PDP treatment, vessels were manually traced, and the ECM-covered area percentage was quantified within a 1 μm zone from the vessel by thresholding. It was found that the ECM-covered area % in the subendothelial space decreased from 36.34 ± 1.71 to 23.08 ± 2.63% at 24 h post-PDP treatment (Figure 5E). Overall, we observed drastic changes in the collagen content at the level of the whole tumor, as well as a decrease in the ECM coverage in the subendothelial zone following PDP. While further studies are needed to validate the connection between the observed changes in the ECM structure and the enhanced nanoparticle extravasation, these findings highlight the importance of elucidating the PDT effects beyond cell killing and vascular modulation.

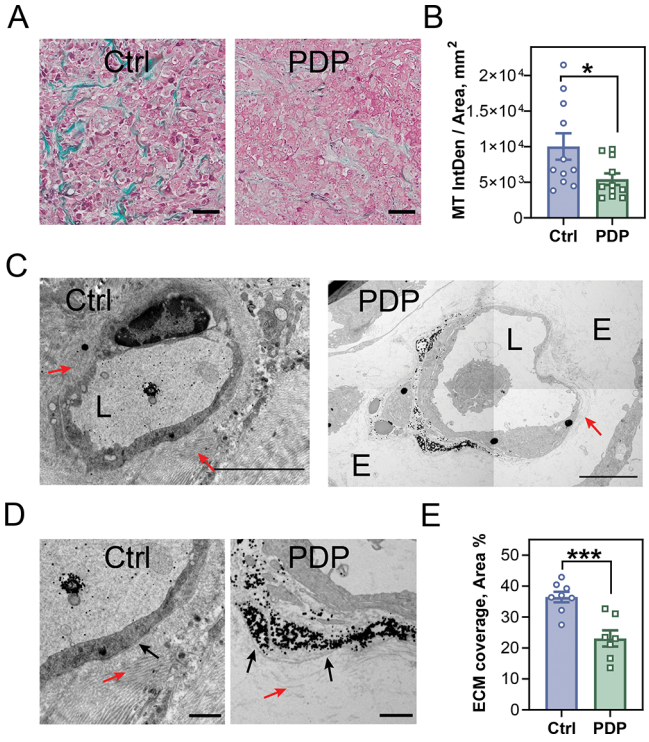

Figure 5. PDP-induced changes in the tumor extracellular matrix content and ultrastructure. (A) Masson's trichrome-stained sections from tumors with and without photodynamic priming, demonstrating a significant reduction in collagen content (blue) 24 h following PDP. Scale bar = 50 μm. (B) Masson's trichrome integrated density was quantified in whole-tumor sections. (C) Representative TEM images of vessels from tumors with and without PDP treatment. L = vessel lumen; E - edema; red arrows - extracellular matrix. Scale bar = 5 μm. (D) Magnified TEM images of the subendothelial area from tumors with and without PDP treatment. Red arrows - extracellular matrix; black arrows - basement membrane. Scale bar = 1 μm (E). Data represented as a mean ± S.E.M., each data point on the graph represents a separate tumor, two-tailed t test, *$P \leq 0.05$; *** $P \leq 0.001$.

CONCLUSIONS

We first demonstrated by using two complementary and independent methods that subtherapeutic photodynamic priming exerts profound effects on the tumor extracellular matrix content and ultrastructure, which may contribute to the enhanced delivery of nanomedicines. These data suggest that the PDP mechanism involves additional factors beyond cell death and vascular modulation that have not yet been elucidated. This finding is particularly impactful for treatment of desmoplastic tumors, such as pancreatic,[46] breast,[47] and lung[48] cancers.[8,38] Furthermore, we showcased how subtherapeutic PDP enables the delivery of a broad spectrum of organic and inorganic nanoparticles, opening multiple avenues for PDP combinations with gene delivery and immunotherapies, as well as nanoparticle-enabled photothermal and photodynamic therapies. Finally, we validated PDP's utility by demonstrating its ability to enhance the therapeutic efficacy of Doxil by ∼3-times, thereby ameliorating its severe off-target toxicities. This study creates a foundation for future mechanistic investigations of PDP effects on the tumor microenvironment, provides the experimental framework for rigorous PDP optimization as well as characterization of a broad spectrum of its biological effects.

https://dx.doi.org/10.1021/acs.nanolett.0c03731
Nano Lett. 2021, 21, 344−352

■ ASSOCIATED CONTENT

Supporting Information

The Supporting Information is available free of charge at https://pubs.acs.org/doi/10.1021/acs.nanolett.0c03731.

Materials and methods as well as BPP characterization, characterization of nanoparticles used in the study, additional Doxil accumulation experiments, and Doxil dose−response study (PDF)

■ AUTHOR INFORMATION

Corresponding Author

Gang Zheng − *Princess Margaret Cancer Centre, University Health Network, Toronto, Ontario M5G 1L7, Canada; Institute of Biomedical Engineering, University of Toronto, Toronto, Ontario M5G 1L7, Canada; Department of Medical Biophysics, University of Toronto, Toronto, Ontario M5G 1L7, Canada;* orcid.org/0000-0002-0705-7398; Email: gang.zheng@uhnres.utoronto.ca

Authors

Marta Overchuk − *Princess Margaret Cancer Centre, University Health Network, Toronto, Ontario M5G 1L7, Canada; Institute of Biomedical Engineering, University of Toronto, Toronto, Ontario M5G 1L7, Canada*

Kara M. Harmatys − *Princess Margaret Cancer Centre, University Health Network, Toronto, Ontario M5G 1L7, Canada*

Shrey Sindhwani − *Institute of Biomedical Engineering, University of Toronto, Toronto, Ontario M5G 1L7, Canada*

Maneesha A. Rajora − *Princess Margaret Cancer Centre, University Health Network, Toronto, Ontario M5G 1L7, Canada; Institute of Biomedical Engineering, University of Toronto, Toronto, Ontario M5G 1L7, Canada*

Adam Koebel − *Department of Pharmaceutical Sciences, Leslie Dan Faculty of Pharmacy, University of Toronto, Toronto, Ontario M5S 3M2, Canada*

Danielle M. Charron − *Princess Margaret Cancer Centre, University Health Network, Toronto, Ontario M5G 1L7, Canada; Institute of Biomedical Engineering, University of Toronto, Toronto, Ontario M5G 1L7, Canada;* orcid.org/0000-0002-1807-6703

Abdullah M. Syed − *J. David Gladstone Institutes, San Francisco, California 94158, USA;* orcid.org/0000-0001-9156-9662

Juan Chen − *Princess Margaret Cancer Centre, University Health Network, Toronto, Ontario M5G 1L7, Canada*

Martin G. Pomper − *Department of Radiology, Johns Hopkins School of Medicine, Baltimore, Maryland 21205, United States;* orcid.org/0000-0001-6753-3010

Brian C. Wilson − *Princess Margaret Cancer Centre, University Health Network, Toronto, Ontario M5G 1L7, Canada; Department of Medical Biophysics, University of Toronto, Toronto, Ontario M5G 1L7, Canada*

Warren C. W. Chan − *Institute of Biomedical Engineering, University of Toronto, Toronto, Ontario M5G 1L7, Canada;* orcid.org/0000-0001-5435-4785

Complete contact information is available at: https://pubs.acs.org/10.1021/acs.nanolett.0c03731

Notes

The authors declare no competing financial interest.

■ ACKNOWLEDGMENTS

The authors would like to acknowledge Mark Zheng, Maartje Damen, and Dr. Miffy Cheng for their assistance with animal experiments. The authors also thank Deborah Scollard, Teesha Komal, and Dr. Manuela Ventura for technical assistance with imaging experiments. Additionally, the authors acknowledge members of STTARR Pathology Core Feryal Sarraf and Napoleon Law and Dr. Vivian Bradaschia from The Centre for Phenogenomics for their pathology services as well as Dr. Ali Darbandi at SickKids Hospital (Toronto) for help in preparing tissue grids for TEM. This study was funded by the Terry Fox Research Institute (PPG#1075), the Canadian Institute of Health Research (Foundation Grant #154326), the Vanier Canada Graduate Scholarship, the Canada Foundation for Innovation (no. 21765), the Natural Sciences and Engineering Research Council of Canada (no. 386613), the Canada Research Chair Programs, the Nanomedicine Innovation Network, and the Princess Margaret Cancer Foundation.

■ REFERENCES

(1) Matsumura, Y.; Maeda, H. A new concept for macromolecular therapeutics in cancer chemotherapy: mechanism of tumoritropic accumulation of proteins and the antitumor agent smancs. *Cancer Res.* **1986**, *46* (12), 6387−92.

(2) Jain, R. K.; Gerlowski, L. E. Extravascular transport in normal and tumor tissues. *Crit Rev. Oncol Hematol* **1986**, *5* (2), 115−170.

(3) Wolfram, J.; Ferrari, M. Clinical Cancer Nanomedicine. *Nano Today* **2019**, *25*, 85−98.

(4) Wilhelm, S.; Tavares, A. J.; Dai, Q.; Ohta, S.; Audet, J.; Harold, F.; Dvorak, H. F.; Chan, W. C. W. Analysis of nanoparticle delivery to tumours. *Nature Reviews Materials* **2016**, *1* (5), 16014.

(5) Walkey, C. D.; Chan, W. C. Understanding and controlling the interaction of nanomaterials with proteins in a physiological environment. *Chem. Soc. Rev.* **2012**, *41* (7), 2780−99.

(6) De Palma, M.; Biziato, D.; Petrova, T. V. Microenvironmental regulation of tumour angiogenesis. *Nat. Rev. Cancer* **2017**, *17* (8), 457−474.

(7) Dewhirst, M. W.; Secomb, T. W. Transport of drugs from blood vessels to tumour tissue. *Nat. Rev. Cancer* **2017**, *17* (12), 738−750.

(8) Henke, E.; Nandigama, R.; Ergun, S. Extracellular Matrix in the Tumor Microenvironment and Its Impact on Cancer Therapy. *Front Mol. Biosci* **2020**, *6*, 160.

(9) Yu, M.; Tannock, I. F. Targeting tumor architecture to favor drug penetration: a new weapon to combat chemoresistance in pancreatic cancer? *Cancer Cell* **2012**, *21* (3), 327−9.

(10) Abyaneh, H. S.; Regenold, M.; McKee, T. D.; Allen, C.; Gauthier, M. A. Towards extracellular matrix normalization for improved treatment of solid tumors. *Theranostics* **2020**, *10* (4), 1960−1980.

(11) Fan, W.; Yung, B.; Huang, P.; Chen, X. Nanotechnology for Multimodal Synergistic Cancer Therapy. *Chem. Rev.* **2017**, *117* (22), 13566−13638.

(12) Nakamura, Y.; Mochida, A.; Choyke, P. L.; Kobayashi, H. Nanodrug Delivery: Is the Enhanced Permeability and Retention Effect Sufficient for Curing Cancer? *Bioconjugate Chem.* **2016**, *27* (10), 2225−2238.

(13) Danhier, F. To exploit the tumor microenvironment: Since the EPR effect fails in the clinic, what is the future of nanomedicine? *J. Controlled Release* **2016**, *244* (Pt A), 108−121.

(14) Overchuk, M.; Zheng, G. Overcoming obstacles in the tumor microenvironment: Recent advancements in nanoparticle delivery for cancer theranostics. *Biomaterials* **2018**, *156*, 217−237.

(15) Dhaliwal, A.; Zheng, G. Improving accessibility of EPR-insensitive tumor phenotypes using EPR-adaptive strategies: Designing a new perspective in nanomedicine delivery. *Theranostics* **2019**, *9* (26), 8091−8108.

(16) van Straten, D.; Mashayekhi, V.; de Bruijn, H. S.; Oliveira, S.; Robinson, D. J. Oncologic Photodynamic Therapy: Basic Principles, Current Clinical Status and Future Directions. *Cancers* **2017**, *9* (12), 19.
(17) Plaetzer, K.; Krammer, B.; Berlanda, J.; Berr, F.; Kiesslich, T. Photophysics and photochemistry of photodynamic therapy: fundamental aspects. *Lasers Med. Sci.* **2009**, *24* (2), 259−68.
(18) Dougherty, T. J.; Gomer, C. J.; Henderson, B. W.; Jori, G.; Kessel, D.; Korbelik, M.; Moan, J.; Peng, Q. Photodynamic therapy. *J. Natl. Cancer Inst* **1998**, *90* (12), 889−905.
(19) Snyder, J. W.; Greco, W. R.; Bellnier, D. A.; Vaughan, L.; Henderson, B. W. Photodynamic therapy: a means to enhanced drug delivery to tumors. *Cancer Res.* **2003**, *63* (23), 8126−31.
(20) Huang, H. C.; Rizvi, I.; Liu, J.; Anbil, S.; Kalra, A.; Lee, H.; Baglo, Y.; Paz, N.; Hayden, D.; Pereira, S.; Pogue, B. W.; Fitzgerald, J.; Hasan, T. Photodynamic Priming Mitigates Chemotherapeutic Selection Pressures and Improves Drug Delivery. *Cancer Res.* **2018**, *78* (2), 558−571.
(21) Zhen, Z.; Tang, W.; Chuang, Y. J.; Todd, T.; Zhang, W.; Lin, X.; Niu, G.; Liu, G.; Wang, L.; Pan, Z.; Chen, X.; Xie, J. Tumor vasculature targeted photodynamic therapy for enhanced delivery of nanoparticles. *ACS Nano* **2014**, *8* (6), 6004−13.
(22) Gao, W.; Wang, Z.; Lv, L.; Yin, D.; Chen, D.; Han, Z.; Ma, Y.; Zhang, M.; Yang, M.; Gu, Y. Photodynamic Therapy Induced Enhancement of Tumor Vasculature Permeability Using an Upconversion Nanoconstruct for Improved Intratumoral Nanoparticle Delivery in Deep Tissues. *Theranostics* **2016**, *6* (8), 1131−44.
(23) Chen, B.; Pogue, B. W.; Luna, J. M.; Hardman, R. L.; Hoopes, P. J.; Hasan, T. Tumor vascular permeabilization by vascular-targeting photosensitization: effects, mechanism, and therapeutic implications. *Clin. Cancer Res.* **2006**, *12* (3), 917−923.
(24) Perentes, J. Y.; Wang, Y.; Wang, X.; Abdelnour, E.; Gonzalez, M.; Decosterd, L.; Wagnieres, G.; van den Bergh, H.; Peters, S.; Ris, H. B.; Krueger, T. Low-Dose Vascular Photodynamic Therapy Decreases Tumor Interstitial Fluid Pressure, which Promotes Liposomal Doxorubicin Distribution in a Murine Sarcoma Metastasis Model. *Transl Oncol* **2014**, *7*, 393−399.
(25) Cavin, S.; Wang, X.; Zellweger, M.; Gonzalez, M.; Bensimon, M.; Wagnieres, G.; Krueger, T.; Ris, H. B.; Gronchi, F.; Perentes, J. Y. Interstitial fluid pressure: A novel biomarker to monitor photo-induced drug uptake in tumor and normal tissues. *Lasers Surg. Med.* **2017**, *49* (8), 773−780.
(26) Cavin, S.; Riedel, T.; Rosskopfova, P.; Gonzalez, M.; Baldini, G.; Zellweger, M.; Wagnieres, G.; Dyson, P. J.; Ris, H. B.; Krueger, T.; Perentes, J. Y. Vascular-targeted low dose photodynamic therapy stabilizes tumor vessels by modulating pericyte contractility. *Lasers Surg. Med.* **2019**, *51* (6), 550−561.
(27) Wang, Y.; Perentes, J. Y.; Schafer, S. C.; Gonzalez, M.; Debefve, E.; Lehr, H. A.; van den Bergh, H.; Krueger, T. Photodynamic drug delivery enhancement in tumours does not depend on leukocyte-endothelial interaction in a human mesothelioma xenograft model. *Eur. J. Cardiothorac Surg* **2012**, *42* (2), 348−54.
(28) Sano, K.; Nakajima, T.; Choyke, P. L.; Kobayashi, H. The effect of photoimmunotherapy followed by liposomal daunorubicin in a mixed tumor model: a demonstration of the super-enhanced permeability and retention effect after photoimmunotherapy. *Mol. Cancer Ther.* **2014**, *13* (2), 426−32.
(29) Sano, K.; Nakajima, T.; Choyke, P. L.; Kobayashi, H. Markedly enhanced permeability and retention effects induced by photoimmunotherapy of tumors. *ACS Nano* **2013**, *7* (1), 717−24.
(30) Kobayashi, H.; Choyke, P. L. Super enhanced permeability and retention (SUPR) effects in tumors following near infrared photoimmunotherapy. *Nanoscale* **2016**, *8* (25), 12504−9.
(31) Kobayashi, H.; Choyke, P. L. Near-Infrared Photoimmunotherapy of Cancer. *Acc. Chem. Res.* **2019**, *52* (8), 2332−2339.
(32) De Silva, P.; Saad, M. A.; Thomsen, H. C.; Bano, S.; Ashraf, S.; Hasan, T. Photodynamic therapy, priming and optical imaging: Potential co-conspirators in treatment design and optimization — a Thomas Dougherty Award for Excellence in PDT paper. *J. Porphyrins Phthalocyanines* **2020**, *24*, 1320−1360.
(33) Lan, G.; Ni, K.; Xu, Z.; Veroneau, S. S.; Song, Y.; Lin, W. Nanoscale Metal-Organic Framework Overcomes Hypoxia for Photodynamic Therapy Primed Cancer Immunotherapy. *J. Am. Chem. Soc.* **2018**, *140* (17), 5670−5673.
(34) Spring, B. Q.; Bryan Sears, R.; Zheng, L. Z.; Mai, Z.; Watanabe, R.; Sherwood, M. E.; Schoenfeld, D. A.; Pogue, B. W.; Pereira, S. P.; Villa, E.; Hasan, T. A photoactivable multi-inhibitor nanoliposome for tumour control and simultaneous inhibition of treatment escape pathways. *Nat. Nanotechnol.* **2016**, *11* (4), 378−87.
(35) Weijer, R.; Clavier, S.; Zaal, E. A.; Pijls, M. M.; van Kooten, R. T.; Vermaas, K.; Leen, R.; Jongejan, A.; Moerland, P. D.; van Kampen, A. H.; van Kuilenburg, A. B.; Berkers, C. R.; Lemeer, S.; Heger, M. Multi-OMIC profiling of survival and metabolic signaling networks in cells subjected to photodynamic therapy. *Cell. Mol. Life Sci.* **2017**, *74* (6), 1133−1151.
(36) Anbil, S.; Pigula, M.; Huang, H. C.; Mallidi, S.; Broekgaarden, M.; Baglo, Y.; De Silva, P.; Simeone, D. M.; Mino-Kenudson, M.; Maytin, E. V.; Rizvi, I.; Hasan, T. Vitamin D Receptor Activation and Photodynamic Priming Enables Durable Low-dose Chemotherapy. *Mol. Cancer Ther.* **2020**, *19* (6), 1308−1319.
(37) Obaid, G.; Bano, S.; Mallidi, S.; Broekgaarden, M.; Kuriakose, J.; Silber, Z.; Bulin, A. L.; Wang, Y.; Mai, Z.; Jin, W.; Simeone, D.; Hasan, T. Impacting Pancreatic Cancer Therapy in Heterotypic in Vitro Organoids and in Vivo Tumors with Specificity-Tuned, NIR-Activable Photoimmunonanoconjugates: Towards Conquering Desmoplasia? *Nano Lett.* **2019**, *19* (11), 7573−7587.
(38) Miao, L.; Lin, C. M.; Huang, L. Stromal barriers and strategies for the delivery of nanomedicine to desmoplastic tumors. *J. Controlled Release* **2015**, *219*, 192−204.
(39) Yokoi, K.; Kojic, M.; Milosevic, M.; Tanei, T.; Ferrari, M.; Ziemys, A. Capillary-wall collagen as a biophysical marker of nanotherapeutic permeability into the tumor microenvironment. *Cancer Res.* **2014**, *74* (16), 4239−46.
(40) Overchuk, M.; Damen, M. P. F.; Harmatys, K. M.; Pomper, M. G.; Chen, J.; Zheng, G. Long-Circulating Prostate-Specific Membrane Antigen-Targeted NIR Phototheranostic Agent. *Photochem. Photobiol.* **2020**, *96*, 718−724.
(41) Cui, L.; Lin, Q.; Jin, C. S.; Jiang, W.; Huang, H.; Ding, L.; Muhanna, N.; Irish, J. C.; Wang, F.; Chen, J.; Zheng, G. A PEGylation-Free biomimetic porphyrin nanoplatform for personalized cancer theranostics. *ACS Nano* **2015**, *9* (4), 4484−4495.
(42) Ng, K. K.; Shakiba, M.; Huynh, E.; Weersink, R. A.; Roxin, A.; Wilson, B. C.; Zheng, G. Stimuli-responsive photoacoustic nanoswitch for in vivo sensing applications. *ACS Nano* **2014**, *8* (8), 8363−8373.
(43) Sykes, E. A.; Chen, J.; Zheng, G.; Chan, W. C. Investigating the impact of nanoparticle size on active and passive tumor targeting efficiency. *ACS Nano* **2014**, *8* (6), 5696−706.
(44) Tannock, I. F.; Lee, C. M.; Tunggal, J. K.; Cowan, D. S.; Egorin, M. J. Limited penetration of anticancer drugs through tumor tissue: a potential cause of resistance of solid tumors to chemotherapy. *Clin. Cancer Res.* **2002**, *8* (3), 878−84.
(45) Nelson, J. S.; Liaw, L. H.; Orenstein, A.; Roberts, W. G.; Berns, M. W. Mechanism of tumor destruction following photodynamic therapy with hematoporphyrin derivative, chlorin, and phthalocyanine. *J. Natl. Cancer Inst* **1988**, *80* (20), 1599−605.
(46) Neesse, A.; Michl, P.; Frese, K. K.; Feig, C.; Cook, N.; Jacobetz, M. A.; Lolkema, M. P.; Buchholz, M.; Olive, K. P.; Gress, T. M.; Tuveson, D. A. Stromal biology and therapy in pancreatic cancer. *Gut* **2011**, *60* (6), 861−8.
(47) Jakubzig, B.; Baltes, F.; Henze, S.; Schlesinger, M.; Bendas, G. Mechanisms of Matrix-Induced Chemoresistance of Breast Cancer Cells-Deciphering Novel Potential Targets for a Cell Sensitization. *Cancers* **2018**, *10* (12), 495.
(48) Fang, S.; Dai, Y.; Mei, Y.; Yang, M.; Hu, L.; Yang, H.; Guan, X.; Li, J. Clinical significance and biological role of cancer-derived Type I collagen in lung and esophageal cancers. *Thorac. Cancer* **2019**, *10* (2), 277−288.

https://dx.doi.org/10.1021/acs.nanolett.0c03731
Nano Lett. 2021, 21, 344−352